JURNAL INFOTEL
VOL. 16, NO. 4, NOVEMBER 2024, PP. 678–694. DOI:10.20895/INFOTEL.V16I4

RESEARCH ARTICLE

Two Omnidirectional Antenna Models for Ship Hull Corrosion Detection Radar System

Hepi Ludiyati[1*], Erika Dwi Jayanti[2], Aqiila Putri Zharfani Ashlah[3], Hanny Madiawati[4], Enceng Sulaeman[5]

[1-5]High Frequency and Microwave Laboratory, Electrical Department, Politeknik Negeri Bandung, Jalan Gegerkalong Hilir Desa Ciwaruga, Kabupaten Bandung Barat, 40559, Indonesia

*Corresponding email: hepi.ludiyati@polban.ac.id

Received: July 21, 2024; Revised: September 16, 2024; Accepted: October 25, 2024.

Abstract: Corrosion in ship hulls, a potential cause of leaks, can be detected using radar systems, where antennas play a critical role. While microstrip antennas are widely used due to their ease of fabrication, their limitations in bandwidth and gain reduce radar detection precision. This study proposes two modified monopole antenna models to address these challenges. The antennas were designed for ship hull corrosion detection and feature a conical parasitic element to enhance gain and bandwidth. The first model employs an upward-directed parasitic cone with a larger diameter, while the second uses a downward-directed cone with a smaller diameter. The cone diameters were calculated based on half the wavelength of the antenna's operating frequencies. PTFE was incorporated between the monopole and the parasitic cone to prevent short circuits. Performance testing involved a vector network analyzer and software-defined radio. Laboratory-scale physical measurements demonstrated that both antennas exhibited omnidirectional radiation patterns. The first model achieved a frequency range of 3904.7–7793.1 MHz, a bandwidth of 3888.4 MHz, and a maximum gain of 10 dBi. The second model operated within 2282.4–3324.1 MHz, with a bandwidth of 1041.7 MHz and a peak gain of 8 dBi. These results indicate that while the first model outperforms the second in bandwidth and gain, both meet the requirements for ship hull corrosion detection in SDR 1, 8,9,11 and 12.

Keywords: omnidirectional, monopole antenna, parasitic cone, radar, software-defined radio, vector network analyzer

 ISSN: 2085-3688; e-ISSN: 2460-0997

1 Introduction

Indonesia, as a maritime country with vast oceans, relies on ships for low-cost transportation. However, insufficient supervision of ship seaworthiness often leads to accidents, primarily due to hull leaks caused by corrosion. Fortunately, radar technology can detect corrosion and assess its damage. Using transmitting and receiving antennas, corrosion detection radar sends electromagnetic waves at a specific frequency toward the ship's hull. The hull reflects these waves, revealing its condition. A uniform reflected wave indicates no corrosion, while weaker amplitudes in certain areas suggest corrosion caused by air bubbles on the hull.

The transmitting antenna on corrosion detection radar for ship hulls is typically unidirectional to provide strong radiation capabilities. In contrast, the receiving antenna is omnidirectional to maximize detection from various directions [1–4]. These references discuss microstrip antennas, a popular choice due to their lightweight, low profile, and conformal design. However, microstrip antennas have limitations, including a narrow bandwidth and low gain.

The Ministry of Communication and Information regulates the frequency range for ship hull corrosion detection radar from HF to SHF [5], as shown in Table 1, with these frequencies detectable by Software-Defined Radio (SDR). HF waves penetrate thick hulls to detect deep corrosion, while SHF waves, with higher energy and rapid amplitude changes, detect surface structures.

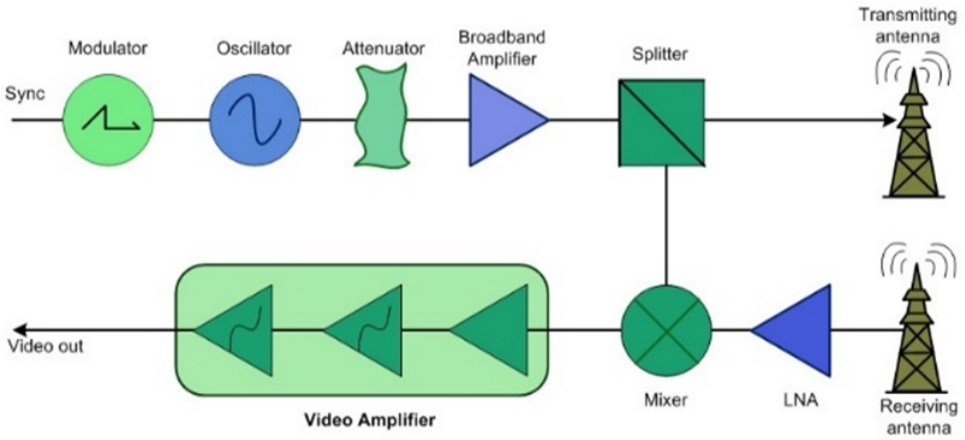

Figure 1: Radar System for Corrosion detection radar for ship hulls.

Omnidirectional antennas, ideal for receiving reflected waves from all directions, are commonly microstrip antennas [6–14]though their low gain and efficiency highlight the need for alternatives like monopole antennas, which offer better power handling [15–17]. Two modified monopole antennas with conical parasitic elements are proposed for SHF wave detection, designed based on half the wavelength of the target frequency range, with further details provided in the Research Method.

Table 1: SDR band frequencies

Channel	Frequency Band (MHz)
SDR 1	1700 - 2000
SDR 2	100 -470
SDR 3	400 - 1700
SDR 4	470 - 800
SDR 6	800 - 1000
SDR 8	2000 - 2300
SDR 9	3200 - 3700
SDR 11	2300 - 2650
SDR 12	2650 - 3200

2 Research Method

2.1 Monopole Antenna

A monopole antenna is a type of wire or rod antenna commonly known as a quarter-wave ($\frac{1}{4}\lambda$) dipole antenna. This antenna is formed by cutting a dipole antenna in half and replacing the missing side with a ground plane [18]. The shape of a monopole antenna can be seen in Figure 2. The physical length of the monopole antenna is closely related to the operating frequency used. The higher the frequency used, the shorter the monopole antenna needed. Therefore, the calculation of the physical length of the monopole antenna is based on the wavelength (λ).

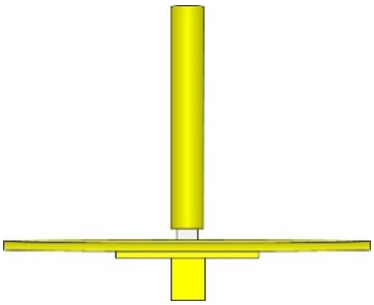

Figure 2: Monopole antenna.

A basic monopole antenna is a type of linear antenna, typically a quarter-wavelength ($\frac{\lambda}{4}$) long (L_m) in a free space (Equation 1 and Equation 2), mounted perpendicular to a ground plane. With the ground as a reflecting plane, it is as if the total length of the monopole antenna is $\frac{1}{2}$ of the wavelength. This condition will result in a maximum electric field right in the middle of the monopole antenna. In Equation 2, f_c (a center frequency in Hz), and c is (3×10^8)m/s as the speed of light. The formula for the radius of a monopole antenna (R_m) often relates to its resonant frequency and wavelength. The formula is derived from transmission line theory or electromagnetic considerations. For a thin wire monopole antenna, the radius (R_m) is often expressed in terms of the resonant wavelength λ, with $R_m \ll \lambda$. For this case, the radius of the monopole antenna is chosen as expressed in Equation 3. This ensures that the antenna behaves properly in terms of impedance matching

and radiation. The ground radius of the monopole antenna is made $\frac{1}{2}$ the wavelength of the free space Equation 4 to produce a maximum electric field magnitude at the center of the ground and zero at both edges of the ground.

For a thin wire monopole antenna, the radius (R_m) is often expressed in terms of the resonant wavelength λ, with $R_m \ll \lambda$. For this case, the radius of the monopole antenna is chosen as expressed in Equation 3. This ensures that the antenna behaves properly in terms of impedance matching and radiation. The ground radius of the monopole antenna is made $\frac{1}{2}$ the wavelength of the free space Equation 4 to produce a maximum electric field magnitude at the center of the ground and zero at both edges of the ground.

$$L_m = \frac{\lambda}{4} \tag{1}$$

$$\lambda = \frac{c}{f_c} \tag{2}$$

$$R_m \leq \frac{\lambda}{20} \tag{3}$$

$$D_g = \frac{\lambda}{2} \tag{4}$$

A basic monopole antenna, typically a quarter-wavelength monopole placed above a ground plane, exhibits an omnidirectional radiation pattern in the horizontal (azimuth) plane. The intensity of the radiation changes with the elevation angle θ. The radiation pattern $E(\theta)$ is like that of a monopole antenna and can be approximated as shown in Equation 5 [19]. The radiation is maximum at $\theta = 90^\circ$ (it means that parallel to the ground plane) and zero at $\theta = 0^\circ$ (directly upward) or $\theta = \pi$ (directly downward).

$$E(\theta) = E_{0\theta} \sin(\theta); 0 \leq \theta \leq 2\pi \tag{5}$$

Where:
$E_{0\theta}$ is the maximum electric field. (volt/meter)
θ is the elevation angle from the zenith.

A quarter-wave monopole antenna positioned over a perfect ground plane has a gain of about 2.15 dBi, which is approximately 3 dB more than a half-wave dipole in free space. This higher gain is a result of the ground plane reflecting the emitted waves, effectively doubling the radiation power. The gain G is related to the directivity D and efficiency η. The relation is shown in 6. For a quarter-wavelength monopole, the directivity is about 5.12 dBi, and with high efficiency ($\eta \approx 1$), the gain is typically around: $G \approx 2.15$dBi. For a more complex design (like adding parasitic elements), the gain will vary based on the geometry.

$$G(dB) = 10log(\eta) + 10log(D) \tag{6}$$

For a basic quarter-wave monopole, the bandwidth (BW) is typically small, but adding matching networks or parasitic elements (as in this case) can widen the bandwidth. The bandwidth is also inversely related to the antenna's quality factor Q, which is dependent on the antenna's electrical size and loading. Quality factors are highly dependent on material loss. The bandwidth is formulated in Equation 7.

$$BW \approx \frac{f_c}{Q} \tag{7}$$

2.2 Parasitic Method

The parasitic method is used in an antenna to increase gain, direct radio waves in a specific direction, and modify the radiation pattern emitted by the main element. Parasitic elements are typically shaped like metal rods or conductors that are not electrically connected to the power source and are located around the active main element [20]. Various shapes can be used for parasitic elements, one of which is a cone. A cone has two circular faces with different diameters. The diameters of the two circles in a cone can vary, with either the base diameter being smaller than the top diameter or vice versa.

To achieve a wide resonance, the wavelength is calculated for the upper and lower limits of the targeted SDR frequency band. To determine the diameters of the cone, the lower frequency (f_l), the upper frequency (f_h), and the center frequency (f_c) are required. The upper frequency is used to calculate the diameter of the smaller circle (D_{p1}), the lower frequency is used to calculate the diameter of the larger circle (D_{p2}), and the center frequency is used to calculate the height of the parasitic element (L_p). The diameters of the cone can be determined using specific equations. Equation 8 is used to find the diameter of the smaller circle (base of the cone). Equation 9 is used to determine the diameter of the larger circle (top of the cone). Equation 10 is used to determine the height of the parasitic element.

$$D_{p1} = \frac{\lambda_h}{2} = \frac{c}{\frac{f_h}{2}} = \frac{c}{2f_h} \tag{8}$$

$$D_{p2} = \frac{\lambda}{2} = \frac{c}{\frac{f_l}{2}} = \frac{c}{2f_l} \tag{9}$$

$$L_p = \frac{c}{2f_c} \tag{10}$$

The selection of the half-wavelength diameter is intended so that the current distribution at the edges of the cone is zero, while at the center of the cone it is maximum.

2.3 Proposed Antennas

The antenna design process is carried out in several steps to ensure it is systematic and structured. The steps of the design process are shown in Figure 3. The predicted characteristics of the proposed antennas were simulated using CST Studio Suites 2019. The dimensions of the proposed antenna construction components, calculated using the previous equations, were incorporated into the simulation setup. In the design of the proposed antennas, the center frequencies for the first model and the second one taken are 2332.38 MHz and 1977.37 MHz, with corresponding wavelengths of 129 mm and 151.72 mm. With these wavelengths, the dimensions, such as the length and diameter of the radiator proposed antennas, are calculated and given in Table 2 and Table 3, respectively.

The materials used were the non-magnetic solid copper sheets magnetic solid copper sheet ($\mu_r = 1, \sigma = 5.8 \times 10^7$ S/m) with thicknesses of 2 mm and 6 mm for the ground plane and radiator, respectively. The impedances of the proposed antennas were calculated and

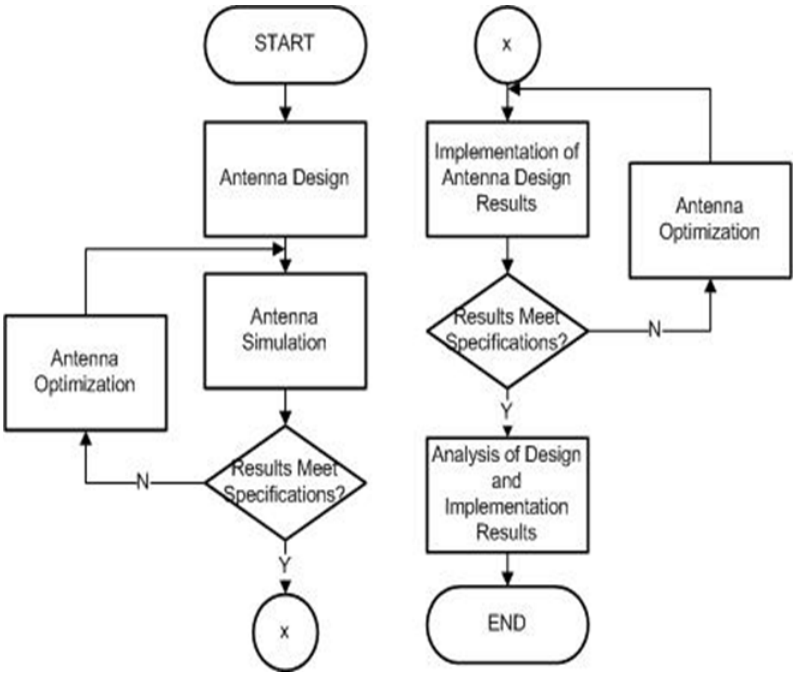

Figure 3: Proposed method.

Table 2: The dimensions of the first model

Dimensions	Value (mm)
Length of monopole antenna (Lm)	37.929
Radius of monopole antenna (Rm)	7.585
Ground plane width of monopole antenna (Gm)	75.85
Top diameter of parasitic element (D_{p1})	65.2
Bottom diameter of parasitic element (D_{p2})	88,2
Length of element parasitic (Lp)	151.717

matched to 50Ω. The geometric structures of the two proposed antenna models are shown in Figure 4 and Figure 5. All parts of the antenna are simulated, including the use of SMA (Small Miniature-A) connectors on the antenna feeders.

The simulated characteristics of the proposed antennas were the S_{11} parameter response as a function of frequency, the gain as a function of frequency, and the radiation patterns at several frequencies. These four parameters represent the main characteristics of a good antenna. CST Studio Suite 2019 software optimizes for frequency values whose impedance produces S_{11} values as required for detecting corrosion on ship hulls. Subsequently, the antenna is prepared in the far field zone to become a directional device that directs electromagnetic wave energy in all directions. From this, the radiation pattern can be determined, including the antenna's gain and radiation efficiency.

Figure 4 and Figure 5 are the proposed antenna structures. In the first model, the parasitic cone is directed upwards, while in the second, it is directed downwards. The first

Table 3: The dimensions of the second model

Dimensions	Value (mm)
Length of monopole antenna (Lm)	35
Radius of monopole antenna (Rm)	6
Ground plane width of monopole antenna (Gm)	2
Top diameter of parasitic element (D_{p1})	85
Bottom diameter of parasitic element (D_{p2})	36
Length of element parasitic (Lp)	7

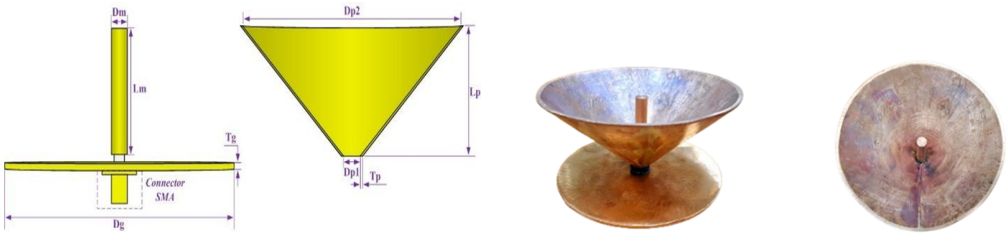

(a) design (b) implementation

Figure 4: Geometry Structure of the first model (the parasitic cone is directed upwards).

monopole rod antenna model includes an upward-facing parasitic cone with a diameter of half the wavelength of the antenna's lower frequency limit. This model is designed to produce a resonance effect in the low-frequency region. The upward-facing cone with a large diameter ensures that the antenna's radiation is equally strong in the horizontal plane (forming a circular pattern) and null at $\theta = 0°$and $\theta = 180°$. The second monopole rod antenna model features a downward-facing parasitic cone. The cone's diameter is half the wavelength of the upper-frequency limit, providing a resonance effect in the high-frequency region. This model also radiates equally in the horizontal plane (forming a circular pattern), but the electric field strength is smaller than that of the first model. In the second model, nulls also occur at $\theta = 0°$and $\theta = 180°$, but with a higher magnitude compared to the first model.

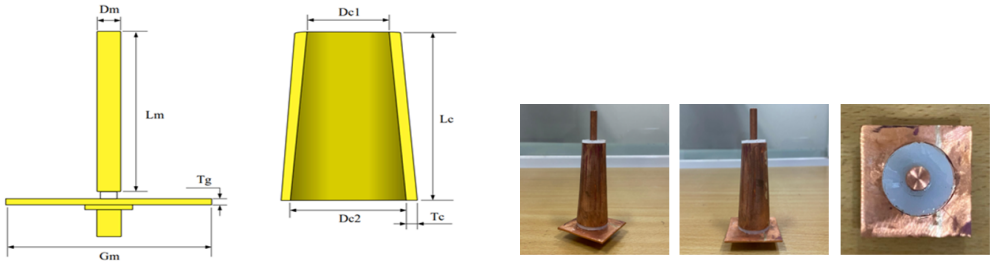

(a) design (b) implementation

Figure 5: Geometry Structure of the second model (the parasitic is directed downwards).

3 Results

3.1 Near Field Parameters

Verification of the simulation results is performed through measurement on a laboratory scale. The physical measurement of antenna characteristics is conducted in a low-interference environment. The measuring instrument used is the Keysight Field Fox Vector Network Analyzer (VNA). The first parameter measured is the near-field parameter, specifically S_{11} as a function of frequency. This parameter can be used as a reference to determine how the antenna input impedance matches the system impedance in the examined frequency range.

The receiving antenna is considered suitable for operation in the frequency range where the $S_{11} \leq -10$ dB, or in other words, where the return loss $RL \geq 10$dB. Under these conditions, the reflected wave between the antenna feeder and the cable is minimized to not exceed 10%. Figure 6 shows the comparison of simulated and measured S_{11} response graphs for the first model. The direct measurement results from the VNA are shown in Figure 7. The antenna works in the dual band, with the 2nd band being wider than the first band. The working frequency range of the first model antenna is shown in Table 3. Referring to the frequency spectrum allocation [5], the working frequency range of the first model antenna meets the requirements for a ship hull corrosion detection radar system (SDR 1, 8, and 9).

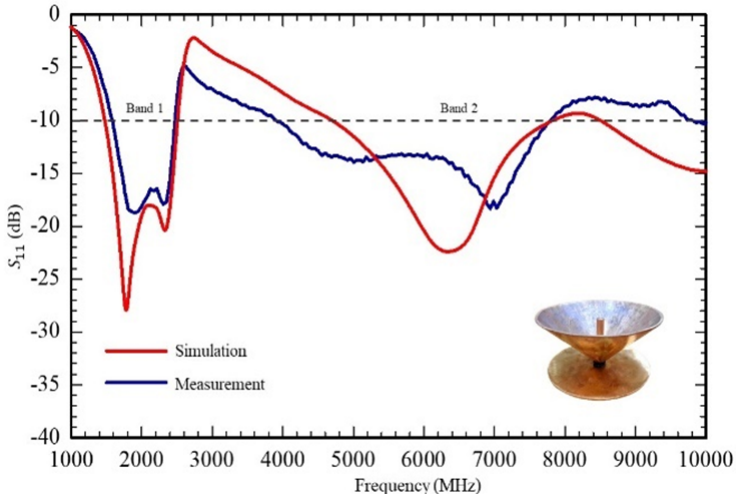

Figure 6: Comparison of simulated and measured S_{11} response graphs for the first model.

For the second model antenna, the frequency function S_{11} curves are shown in Figure 8 and Figure 9. Like the first model antenna, this antenna is also capable of producing a working frequency that meets the requirements for corrosion detection radar (SDR 11 and 12). Detailed working frequencies of the antenna can be seen in Table 4. The simulation and measurement results differ due to several factors, namely imperfection of connector installation, cable loss, and inaccuracy of size due to handmade and material quality.

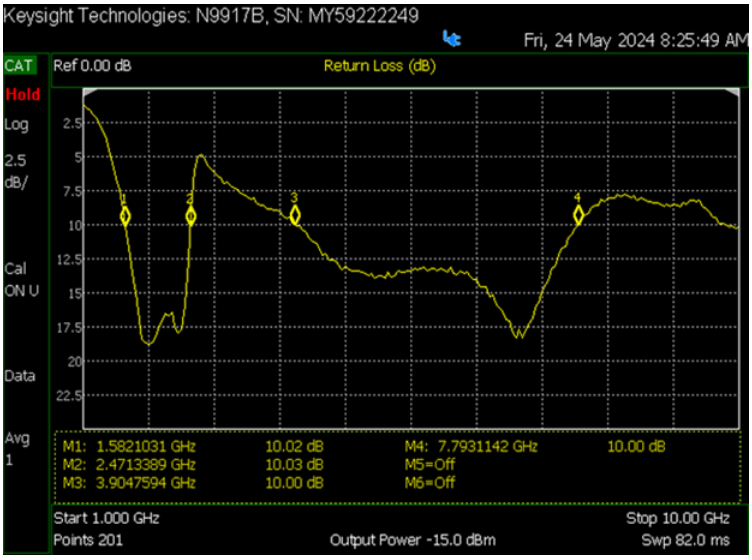

Figure 7: S_{11} Antenna measurement results from VNA for $RL \geq 10$dB for the first model.

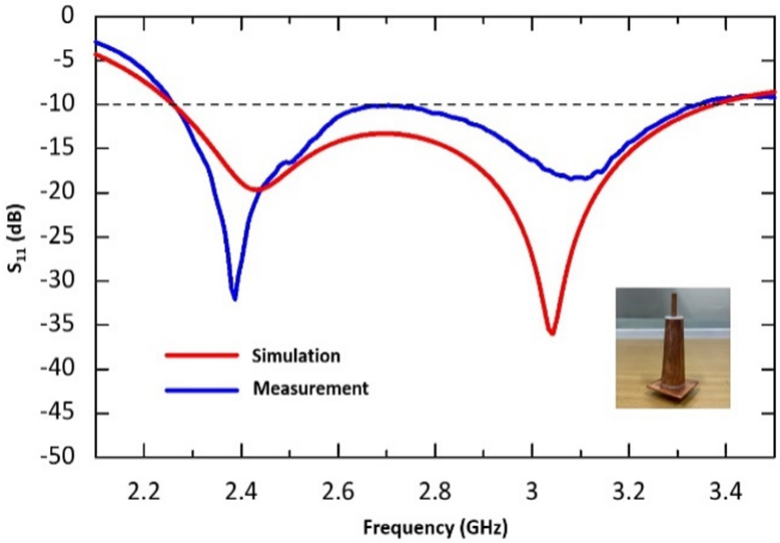

Figure 8: Comparison of simulated and measured S_{11} response graphs for the second model.

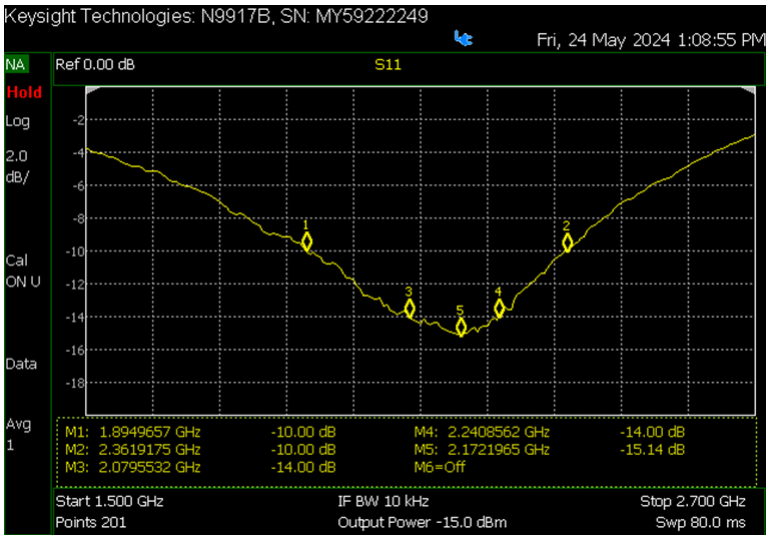

Figure 9: S_{11} Antenna measurement results from VNA for $R \geq 10$ dB for the second model.

Table 4: Comparison of simulated and measured S_{11} response for the first model

Spec.	Simulation		Measurement	
	Band 1	Band 2	Band 1	Band 2
f_l (MHz)	1476.8	4700	1582.1	3904.7
f_h (MHz)	2507.7	7823.6	2471.3	7793.1
BW (MHz)	1030.9	3123.6	889.2	3888.4

3.2 Far Field Parameters

The far-field parameters of the antenna show the characteristics of the antenna in free space. In the case of corrosion detection radar, this means the ability of the antenna to receive reflected waves from the ship's hull with sufficient power to be then interpreted into an image showing the condition of the ship's body. The parameters included in the far field are the radiation pattern and gain. Far-field parameter testing was conducted only on a laboratory scale, not in a real environment, as it requires an actual corrosion detection radar system. Both antenna models produce an omnidirectional radiation pattern, as shown in Figure 10 and Figure 11. These are characterized by "a circle shape" for the top view and "an eight shape" for the side view. The radiation of both omnidirectional antennas is very necessary for the comprehensive detection of corrosive objects on the hull of a ship.

Table 5: Comparison of simulated and measured S_{11} response for the second model

Spec.	Simulation Band 1	Measurement Band 1
f_l (MHz)	2259.3	2282.4
f_h (MHz)	3376.1	3324.1
BW (MHz)	1116.8	1041.7

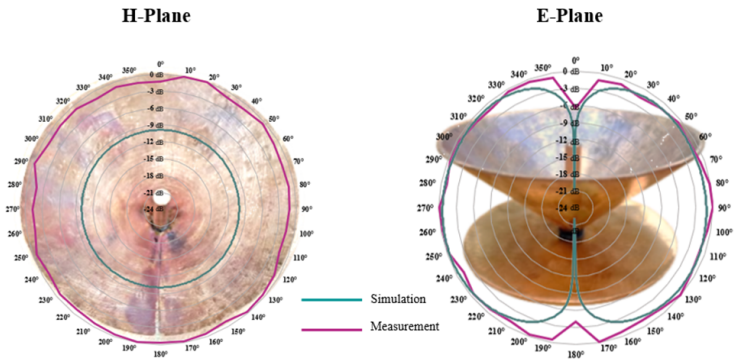

(a) band 1

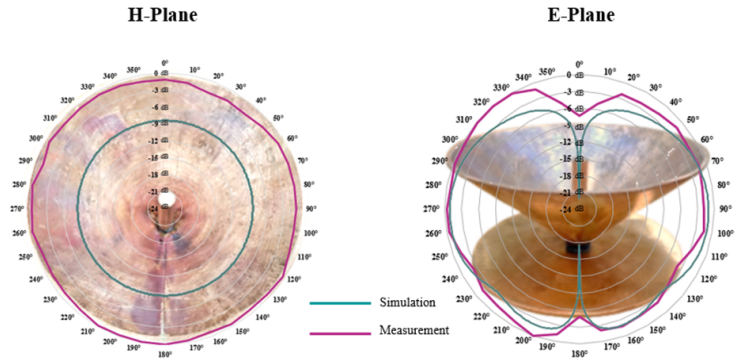

(b) band 2

Figure 10: Radiation patterns for the band 1 and band 2 of the first model.

An illustration system of radar applications to detect ship hull corrosion is shown in Figure 12. The radar system is mounted on a drone, and its weight is calculated. Based on an experiment on a laboratory scale, for detection purposes, the antenna needs a gain of at least 5 dBi. At this gain level, 5 dB of radar wave energy is focused on the ship's structure. The gain produced by both antenna models varies with frequency. For the first model, the green line represents simulated gain, the red line represents horizontal position gain, and the purple line represents vertical position gain, as shown Figure 13 to Figure 14.

The simulation gain is smaller than the measurement gain because in the simulation, the radar wave source is not generated in the test frequency area. In contrast, in the measurements, it is used at the test frequency with a power level of 0 dBm. For the detection corrosion function of the first model antenna in the far field region, tests were carried out using a signal generator set to 0 dBm at a frequency of 4.8 GHz. At this frequency, the antenna gain is 4 dBi. The distance between the transmitter and receiver is more than 2 meters. With the path loss generated at the test frequency for more than 2 meters, the first model antenna was able to receive a power of -49.67 dBm (see Figure 16). The second model antenna, tested at 3.6 GHz with the same transmit power and distance, received

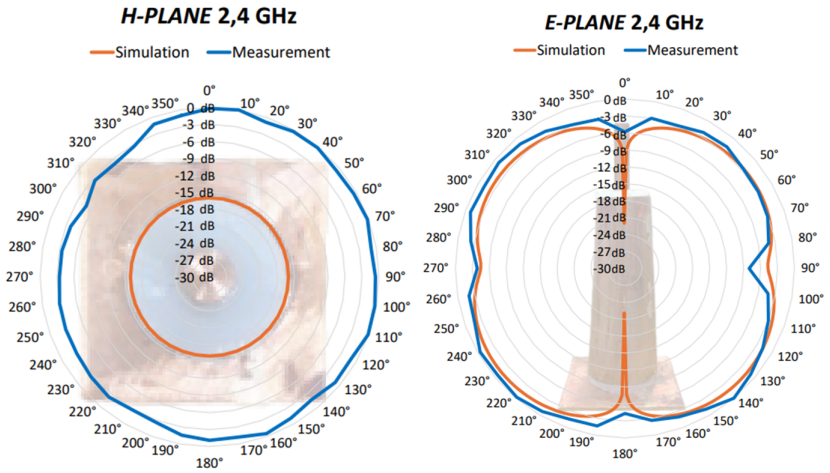

Figure 11: Radiation pattern for the second model.

Figure 12: Illustration system of radar applications to detect ship hull corrosion.

-47.78 dBm. Both antenna models have a gain of more than 4 dBi at their respective test frequencies. For the second model, we present it in different colors (see Figure 15).

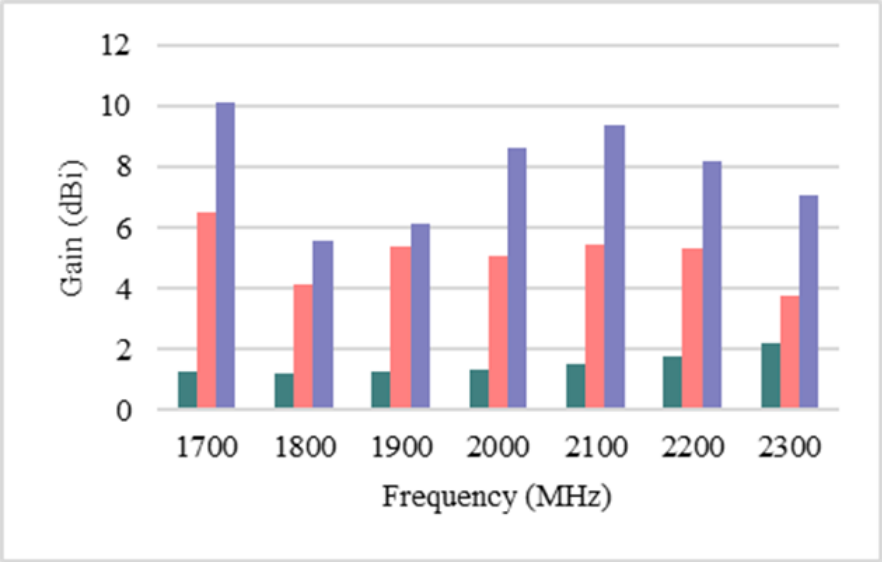

Figure 13: Comparison of simulated (green) and measured gain (red = vertical, purple = horizontal) on the first band.

However, path loss is higher at 4.8 GHz compared to 3.6 GHz. This explains why the first model antenna received less power (-49.67 dBm) than the second (-47.78 dBm) (see Figure 17). With varying gain from 4 dBi to 10 dBi and maximum omnidirectional polarization in the phi plane, both proposed antenna models are predicted to be able to perform corrosion detection functions. The power received by both antennas is quite low due to the unavoidable path loss.

4 Discussion

In this section, important results from research on the comparison of the characteristics of two modified monopole antenna models will be discussed to gain more attention. First, the parasitic elements have worked well. The addition of parasitic cone-shaped elements to the main antenna has been able to expand the widest bandwidth to 3888.4 MHz and 1041.7 MHz. In addition, parasitic elements are able to increase the largest main antenna gain up to 10 dBi. However, the addition of parasitic elements does not change the radiation pattern of the main antenna. Monopole antennas have omnidirectional radiation polarization, and after adding parasitic elements, they remain omnidirectional. Antenna designs using copper plates can be recommended for antennas with detection functions. Apart from good power handling capacity, antennas made from this material can also produce good performance for radar applications to detect ship hull corrosion in SDR 1, 8, 9, 11, and 12.

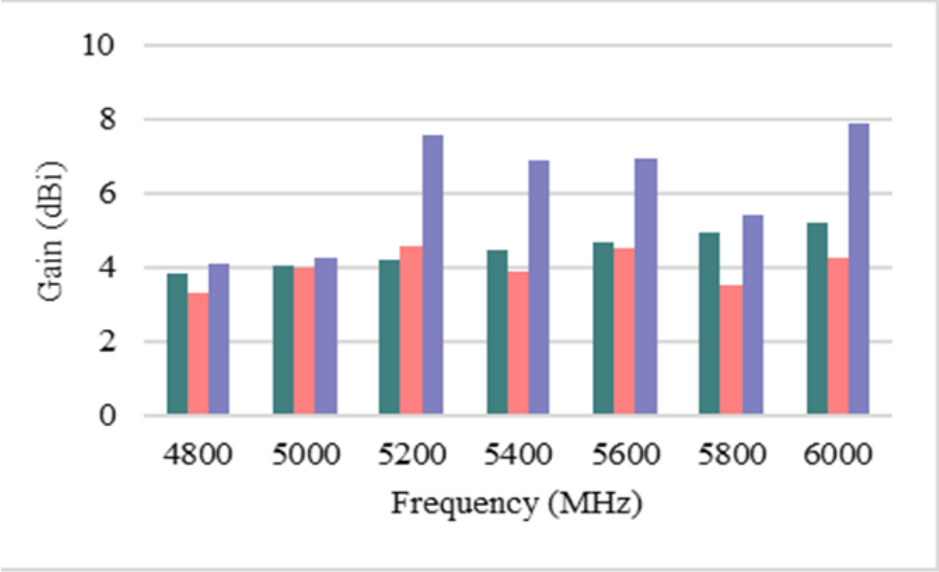

Figure 14: Comparison of simulated and measured gain on the second band.

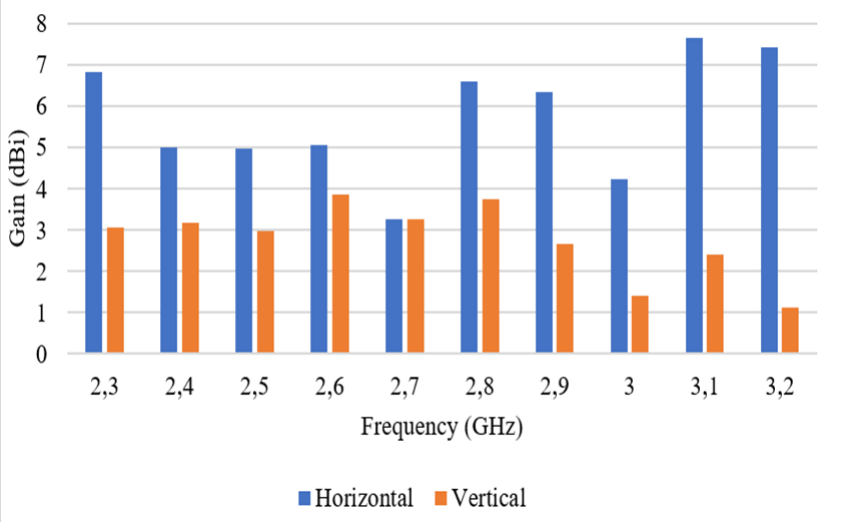

Figure 15: Measured gain of the second model.

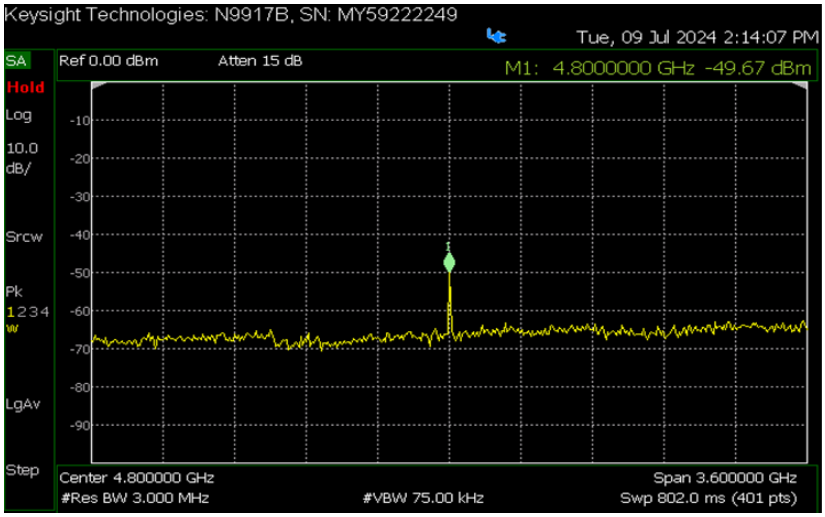

Figure 16: Power received by the first model antenna at the 4.8 GHz frequency.

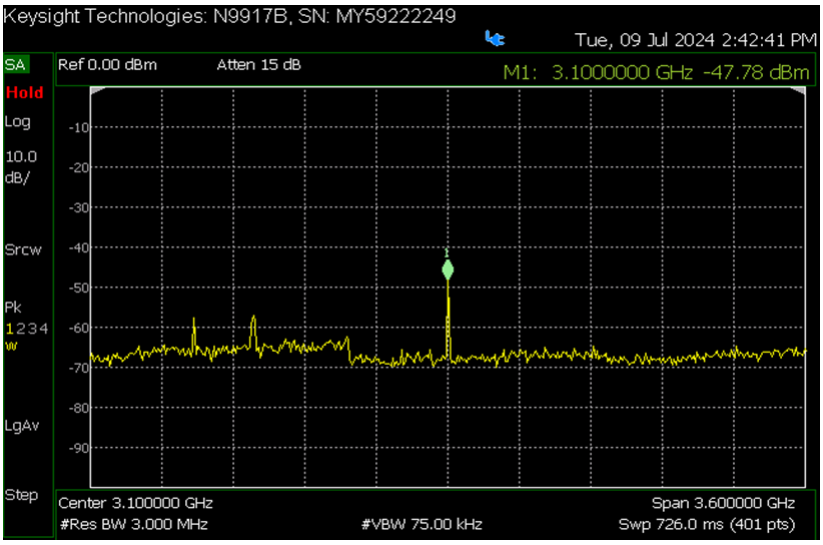

Figure 17: Power received by the second model antenna at the 3.1 GHz frequency.

5 Conclusion

This research successfully designed and tested two modified monopole antenna models for ship hull corrosion detection, with performance measurements conducted on a laboratory scale. The first model, featuring an upward-facing conical parasitic element, achieved a broader bandwidth of 3888.4 MHz (3904.7 MHz to 7793.1 MHz) and a higher gain of 10 dBi. The second model, with a downward-facing cone, operated in the 2282.4 MHz to 3324.1 MHz range, providing a bandwidth of 1041.7 MHz and a gain of 8 dBi. A PTFE layer was added in the second model to prevent short circuits. Both models demonstrated omnidirectional radiation patterns during laboratory testing. While the first model exhibited superior performance in terms of bandwidth and gain, both antennas meet the necessary criteria for detecting ship hull corrosion, offering promising solutions for radar applications in maritime environments.

Acknowledgments

We would like to thank the Head of the Center for Research and Community Service at Bandung State Polytechnic (Politeknik Negeri Bandung) for providing funds for applied research through Contract Letter No. B/3.13/PL1.R7/PG.00.03/2024.

References

[1] C. Sun, N. Du, Y. Guo, X. Zhang, H. Zhang, and X. Ye, "A compact magneto-electric dipole antenna for s-band MIMO through-wall radar," *IEEE Access*, vol. 12, pp. 67209–67218, 2024.

[2] L. Zhu, J. Sun, G. Xu, Z. Hao, and Q. Cao, "An integrated antenna array with broadband, low-RCS, and high-gain characteristics," *IEEE Trans. Antennas Propag.*, vol. 72, pp. 5408–5413, June 2024.

[3] C. Hua, J. Liu, Y. Yu, W. Ren, and Z. Shen, "Low-profile and wideband surface-wave antenna of conical beam for uav applications," *IEEE Antennas and Wireless Propagation Letters*, vol. 23, p. 1548–1552, May 2024.

[4] Y.-S. Huang, D.-X. Ni, L. Zhou, Z. Zhao, C.-R. Zhang, S. Wang, Y. Xie, R.-Q. Liu, and J.-F. Mao, "A 1t2r heterogeneously integrated phased-array fmcw radar transceiver with amc-based antenna in package in the w-band," *IEEE Transactions on Microwave Theory and Techniques*, vol. 72, p. 3772–3787, June 2024.

[5] G. Zheng and B. Sun, "High-gain normal-mode omnidirectional circularly polarized antenna," *IEEE Antennas and Wireless Propagation Letters*, vol. 17, p. 1104–1108, June 2018.

[6] J. Wang, L. Zhao, Z.-C. Hao, and J.-M. Jin, "A wideband dual-polarized omnidirectional antenna for base station/wlan," *IEEE Transactions on Antennas and Propagation*, vol. 66, p. 81–87, Jan. 2018.

[7] L. Zhao, Z.-M. Chen, and J. Wang, "A wideband dual-polarized omnidirectional antenna for 5g/wlan," *IEEE Access*, vol. 7, p. 14266–14272, 2019.

[8] Y. Cui, C. Qi, and R. Li, "A low-profile broadband quad-polarization reconfigurable omnidirectional antenna," *IEEE Transactions on Antennas and Propagation*, vol. 67, p. 4178–4183, June 2019.

[9] J. Cui, A. Zhang, and X. Chen, "An omnidirectional multiband antenna for railway application," *IEEE Antennas and Wireless Propagation Letters*, vol. 19, p. 54–58, Jan. 2020.

[10] S. Wen, Y. Xu, and Y. Dong, "A low-profile dual-polarized omnidirectional antenna for lte base station applications," *IEEE Transactions on Antennas and Propagation*, vol. 69, p. 5974–5979, Sept. 2021.

[11] Z. Wang, Y. Ning, and Y. Dong, "Hybrid metamaterial-tl-based, low-profile, dual-polarized omnidirectional antenna for 5g indoor application," *IEEE Transactions on Antennas and Propagation*, vol. 70, p. 2561–2570, Apr. 2022.

[12] X. Zhai, S. Yan, B. Wang, and J. Zhang, "A low-profile broadband dual-polarized omnidirectional antenna for lte applications," *IEEE Antennas and Wireless Propagation Letters*, vol. 22, p. 1696–1700, July 2023.

[13] S. Yan, X. Zhai, H. Ren, and J. Zhang, "A low-profile dual-polarized omnidirectional antenna for wlan/uwb applications," *IEEE Antennas and Wireless Propagation Letters*, vol. 23, p. 1433–1437, May 2024.

[14] Y.-T. Li, X.-L. Yang, Z.-B. Li, L. Wang, and H.-C. Yang, "A unidirectional cylindrical conformal monopole antenna designed for impulse radar system," *IEEE Antennas and Wireless Propagation Letters*, vol. 10, p. 1397–1400, 2011.

[15] H.-Y. Liang, H.-C. Yang, and J. Zhang, "A cylindrical conformal directional monopole antenna for borehole radar application," *IEEE Antennas and Wireless Propagation Letters*, vol. 11, p. 1525–1528, 2012.

[16] L. Sang, J. Xu, Z. Liu, Y. Mei, W. Wang, and Z. Shen, "Low-rcs uwb planar monopole array antenna based on the optimized design of the conductor layers," *IEEE Transactions on Antennas and Propagation*, vol. 71, p. 3683–3688, Apr. 2023.

[17] W. Kang, S. Yang, K. Kim, C. Kim, and S.-J. Cho, "A cylindrical antenna with a conductively loaded slot for broadband imaging radar applications," *IEEE Transactions on Antennas and Propagation*, vol. 70, p. 10355–10364, Nov. 2022.

[18] D. Jang, N. K. Kong, and H. Choo, "Design of an on-glass 5g monopole antenna for a vehicle window glass," *IEEE Access*, vol. 9, p. 152749–152755, 2021.

[19] C. A. Balanis, "Antenna theory," 2005.

[20] L. Zhao, H. Zhu, H. Zhao, G. Liu, K. Wang, J. Mou, W. Zhang, and J. Li, "Design of wideband dual-polarized me dipole antenna with parasitic elements and improved feed structure," *IEEE Antennas and Wireless Propagation Letters*, vol. 22, p. 174–178, Jan. 2023.